Marine Pollution Bulletin 178 (2022) 113554

Contents lists available at ScienceDirect

Marine Pollution Bulletin

journal homepage: www.elsevier.com/locate/marpolbul

A large-scale study of microplastic abundance in sediment cores from the UK continental shelf and slope

A.T. Kukkola [a,b], G. Senior [a], T. Maes [c], B. Silburn [d], A. Bakir [d], S. Kröger [d], A.G. Mayes [e,*]

[a] School of Environmental Sciences, University of East Anglia, Norwich Research Park, Norwich, NR4 7TJ, UK
[b] School of Geography, Earth and Environmental Sciences, University of Birmingham, B15 2TT, UK
[c] GRID-Arendal, Teaterplassen 3, 4836 Arendal, Norway
[d] Centre for Environment Fisheries and Aquaculture Science, Pakefield Road, Lowestoft NR33 0HT, UK
[e] School of Chemistry, University of East Anglia, Norwich Research Park, Norwich NR4 7TJ, UK

ARTICLE INFO

Keywords:
Nile red
Plastic pollution
Microplastic identification
Microplastic mapping
Low-cost method
Fluorescence

ABSTRACT

To inform risk assessments, reliable, time efficient and affordable quantification methods are required for creating a microplastic (MP) pollution baseline in the world's oceans. To facilitate this, MP abundance was investigated in sediments of three contrasting areas of the UK continental shelf: North West of Jones Bank, the Canyons in the Celtic Sea and Dogger Bank in the North Sea, utilising the Nile Red tagging method to assess its time efficiency and cost. Average MP abundance in the top 10 cm was 1050–2700 MP kg^{-1}. MP abundance decreased with increasing sediment depth and increased with increasing water depth. The findings emphasise the extent of MP pollution and illustrate the value of Nile Red for large scale mapping at relatively low cost.

1. Introduction

Research into microplastics (MPs) and their potential environmental effects has grown exponentially over the past decade, as awareness of the issue has increased. The presence of MPs has been reported around the globe, and in a vast array of environmental compartments, from remote mountain tops to deep oceans (Allen et al., 2021; Cunningham et al., 2020; Cutroneo et al., 2022; Napper et al., 2020). The global ubiquity of MPs, in combination with reports that a variety of organisms ingest them (Besseling et al., 2015; Krause et al., 2021; Kukkola et al., 2021; Maes et al., 2020; Setälä et al., 2014) has raised concerns over their environmental and health effects (Wang et al., 2019b; Zhang et al., 2020). Indeed, MPs are recognised as a threat at the highest levels of governance, through UN SDG 14 (sustainable use of the oceans) and the Marine Strategy Framework Directive (MSFD, 2008/56/EC) in the European Union (EU). In the United States of America (USA), usage of MP beads has been banned in rinse-off cosmetic products by the Microbead-Free Waters Act of 2015 and the United Kingdom in 2018 (UK) has banned MP beads in rinse-off products (Gov.UK press release 19th June 2018). The G7 nations have also introduced the Ocean Decade Navigation plan and the European Chemicals Agency (ECHA) has released a dossier recommending the ban of intentionally added MPs from a range of industrial products (ECHA, 2019), highlighting the urgency surrounding this issue.

To set standards for environmental status, as required by the MSFD 2008/56/EC, a baseline for MP abundance in the marine environment is required, against which future trends can be monitored. In order to obtain a baseline for global environments, much more extensive datasets of MP abundance in the marine environment, representing a diverse range of hydrological conditions, need to be obtained. Marine sediments have been shown to be a stable sink, acting as a hotpot for MP accumulation (Harris, 2020; Maes et al., 2017b). To facilitate the generation of this data in a meaningful timeframe, it will be necessary to collect, process and analyse large numbers of sediment samples in a rapid, accessible and affordable manner.

At present, methods for determining MP abundance in sediments usually involve an extraction step via density separation, which is frequently carried out using a saturated NaCl solution (1.2 g/cm^3) (despite this being inadequate to float denser plastics, such as PET 1.34–1.40 g/cm^3 and PVC 1.38–1.70 g/cm^3), followed by visual identification under brightfield illumination. However, visual identification is highly dependent on subjective understanding of how MPs appear under a light microscope (often based on their colour and shape). Factors such as biofouling and weathering can influence the visual identification rate. According to Löder et al. (2015), spectroscopy has shown that only 1% of particles visually identified as MPs were synthetic

* Corresponding author.
E-mail address: Andrew.mayes@uea.ac.uk (A.G. Mayes).

https://doi.org/10.1016/j.marpolbul.2022.113554
Received 27 September 2021; Received in revised form 4 March 2022; Accepted 8 March 2022
Available online 4 April 2022

polymers. In addition, visual identification is extremely time consuming and requires consistency of personnel throughout to gain some measure of objectivity, and is extremely challenging for small particles. Many studies have turned to vibrational spectroscopy (micro FT-IR or Raman) to positively identify MPs and their polymer type (Araujo et al., 2018; Löder et al., 2015; Vianello et al., 2013), but this comes with the caveats of being very slow (several hours per sample), expensive and requiring complex and demanding instrumentation, only available in a few laboratories and very rarely in developing countries (Nel et al., 2021), where plastic waste problems are most evident. To quantify MPs in the vast number of environmental samples anticipated to satisfy future statutory and regulatory monitoring obligations, a method that does not rely solely on the visual identification of putative MPs is needed. The spectroscopic methodology is highly effective for definitive identification in small numbers of samples and valuable for validation and quality control, but for broad spatial mapping studies and routine monitoring, a different philosophy and approach is required.

Nile Red staining has been proposed to overcome these issues (Erni-Cassola et al., 2017; Maes et al., 2017a; Shim et al., 2016; Shruti et al., 2022; Sturm et al., 2021). These methods take advantage of the characteristic of Nile Red to fluoresce in hydrophobic environments and its tendency to adsorb onto polymer surfaces, due to their lipophilic nature, giving them a fluorescent tag that can be observed under blue light. When combined with density separation, it can reduce the time and effort necessary for the identification of MPs (Maes et al., 2017a). This technique was optimised and validated for marine sediments and has since been used successfully in environmental samples (Bakir et al., 2020a; Bakir et al., 2020b; Patchaiyappan et al., 2021; Preston-Whyte et al., 2021; Tamminga et al., 2018; Valine et al., 2020).

The aim of the present study was to (1) evaluate the operational value of a Nile Red method (Maes et al., 2017a) for a larger scale environmental sample pool. (2) To quantify and compare MP contamination, in three-dimensional detail, from three separate and hydrologically distinct regions of the UK continental shelf (less than 200 m deep) and slope (greater than 200 m depth) (Kröger et al., 2018). Sediment samples were collected during several research cruises on board the RV Cefas Endeavour, from the North-East area of the European continental shelf at Celtic Sea areas of North West of Jones Bank (NWJB) and submarine canyons (CNYN), as well as the shallower area of Dogger Bank (DB) in the central North Sea. Sub-tidal sediments are rarely collected in a manner that preserves the vertical sediment profile, due to the demanding sampling requirements. This study reports a rare example where the vertical resolution of MPs in sediment cores has been maintained during sample collection and analysed in detail for discrete depths. It is, to the best of our knowledge, the first largest-scale depth-profiled MP study at Celtic and North Sea sites, utilising the rapid screening technique with Nile Red (Maes et al., 2017a), and one of the world's first where samples were collected directly from the continental slope. As such, it contributes valuable information regarding MP abundance and provides pointers to the likely factors driving MP abundance and distribution in the marine environment. In this regard, this study aimed to explore whether MP abundance varies with sediment depth, and whether physical characteristics such as water depth have any effect on the MP abundance in sediments.

2. Materials and methods

Sediment cores ($n = 22$) used in this study were collected on the RV Cefas Endeavour from 7th to 16th January, and 20th May to 15th June 2017 by the Centre for Environment, Fisheries and Aquaculture Science (Cefas) as a part of integrated monitoring pilot surveys, or Sentinel Monitoring (type-1) cruises (cruise codes CEND01/17 and CEND09/17) (Murray et al., 2017; Eggett et al., 2018). MP sample collection was opportunistic, carried out alongside the wider survey aims, hence sites were not selected based on MP-driven hypotheses. Cores were collected from three locations; one in the North Sea: DB ($n = 13$), and two sites in the Celtic Sea: NWJB ($n = 6$) and CNYN ($n = 3$) (Fig. 1), the physical parameters of the cores are listed in Table S1. Site selection at each location was governed by the primary survey monitoring aims, as laid out in the cruise reports (Eggett et al., 2018; Murray et al., 2017) with all monitoring stations visited cored for MPs on CEND01/17, while a 10% subset of monitoring stations samples for other parameters were cored for MPs on CEND09/17. All locations are designated as Special Areas of Conversation under the Convention for the Protection of the Marine Environment of the North-east Atlantic (OSPAR) and as such are of particular interest for marine policy development or management considerations. Further details of the broader sampling route selection and rationale have been described in Noble-James et al. (2018).

DB is a large sandbank located in the North Sea, approximately 150 km North-East of the Humber Estuary. Depth ranges between 18 and 50 m. Water masses from the north and south-central North Sea converge at DB (Nielsen et al., 1993). Owing to its open sea location, it is subject to high wave energy (JNCC, 2011) and sediment is thought to be derived from the weathering of Pleistocene formations (Diesing et al., 2009). Sea bed sediments are mostly fine sands, becoming muddy sands in deeper areas (Kröncke and Knust, 1995).

NWJB is an offshore Marine Conservation Zone (MCZ) and is situated on the continental shelf, approximately 165 km west of England's South-West coast and 200 km from Ireland's South coast. The depth at NWJB ranges between 100 and 200 m (Eggett et al., 2018). The sediment types of the NWJB consist of subtidal sand, mixed sediments, coarse sediment and mud (JNCC, 2017).

CNYN (MCZ) is located at the south-west corner of the UK continental shelf boundary, approximately 360 km from England's South-West coast. It is characterized by sub-marine canyons and sharp changes in depth, as it drops from depths of 100 m to depths of 2000 m at the oceanic abyssal plain (JNCC, 2013). This is accompanied by underwater streams that move from shallow to deeper sea areas and near bottom currents carrying nepheloid layers of particulate material (Wilson et al., 2015). All of the cores collected at the CNYN were from depths greater than 200 m, which can be considered as the boundary of the continental shelf (Kröger et al., 2018). The sediment types are dominated by coral rubble, coarse sediment, mud, and sand.

Sediment samples were collected using a 0.08m^2 NIOZ box corer (Eggett et al., 2018), a metal corer which encases the sediment sample and overlying bottom water, and retains it upright throughout the recovery process, enabling the sediment surface to remain undamaged and undisturbed until further sampling (Silburn, 2018; Thompson et al., 2017). Sampling for MP cores was conducted via pushing a pre-cleaned 33 cm long and 5 cm diameter, circular stainless-steel tube into the recovered sediment core until fully inserted (resulting surface area of the individual sub-cores of ~0.00196m^2), the sub-sampling map has been provided in Fig. S2. These cores were then capped with black PE caps and cling film (hence forward "sediment cores") and frozen upright at −18 °C in their steel tubing. The frozen sediment cores were transported to the University of East Anglia, Norwich, United Kingdom, where they remained frozen until processing in a clean laboratory.

Contamination avoidance is essential for meaningful MP analysis and steps were taken to minimise external MP contamination. All working surfaces and equipment were cleaned before and between any processes. All equipment used, where feasible, were made of glass, and during processing samples were kept covered with glass lids. Staff wore 100% cotton laboratory coats and avoided synthetic clothing. All reactants were filtered through 0.2 μm Nylon filters prior to use. Procedural blanks were run over the course of the study. The contamination was found to be non-systematic (~58.8% of the blanks had no contamination present) and where present, approximately 0.6 particle/filter ($n = 17$, SE = 0.3). No fibres were detected on any of the laboratory blanks. The Limit of Detection (LoD) was defined as 3 × the Standard Deviation (SD) of the blank results and was determined to be 3.0 particles per filter. The Limit of Quantification (LoQ) was defined as 3.3 × LOD or 10 × SD of the blank results and was 10.2 particles per filter,

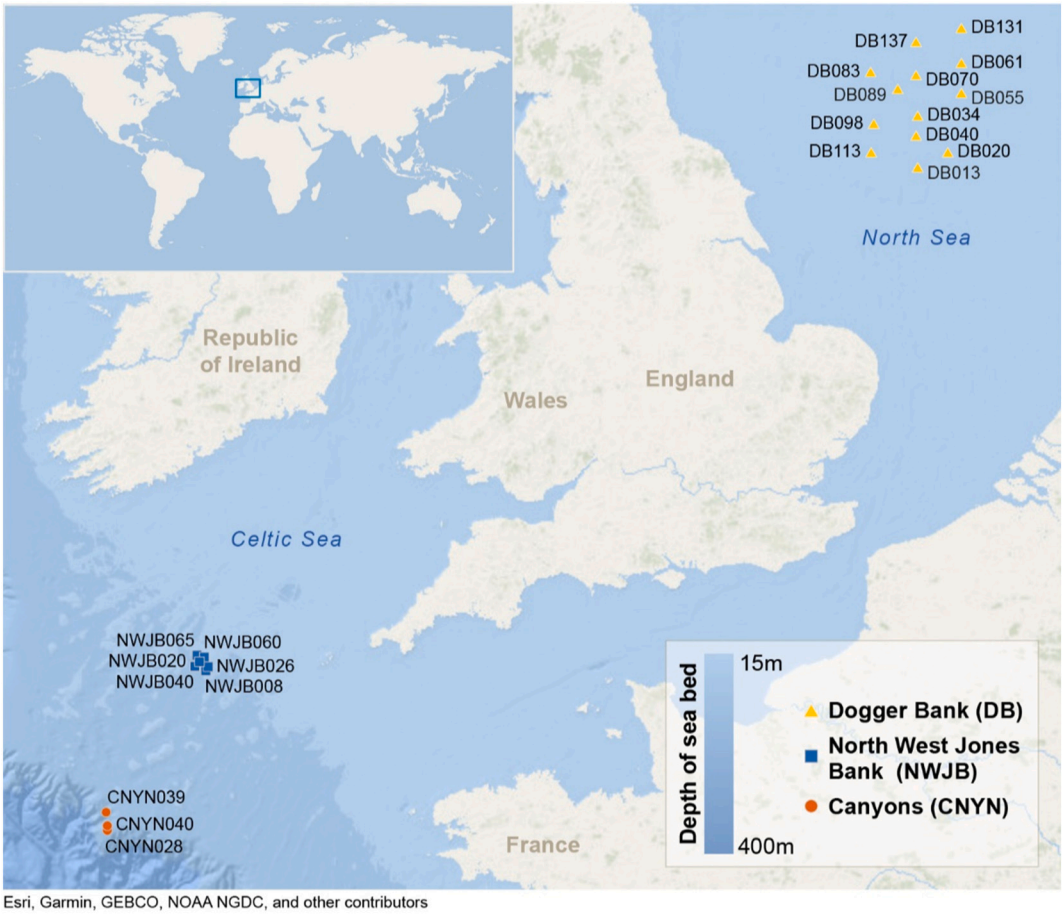

Fig. 1. Geographical and bathymetric context of sampling locations. Symbols: Dogger Bank (DB): yellow triangle, North West Jones Bank (NWJB): blue square and The Canyons (CNYN): orange circle. (For interpretation of the references to colour in this figure legend, the reader is referred to the web version of this article.)

giving the results medium to high significance (Maes et al., 2020).

The blank mean was not subtracted for the statistical analysis from the final MP counts, as it would have provided negative counts in some instances. It has however, been considered in the interpretation of the results.

Sediment cores were defrosted at room temperature and sediment extraction was undertaken using a custom-made tool constructed from wood and aluminum (Fig. S1). The top 5 cm of each core was sliced into 1 cm deep horizons, and the rest was sliced at 2.5 cm intervals. Sediment slices were weighed into glass Petri dishes, placed in a vacuum oven, and dried at a temperature of 40 °C with a continuous bleed of 0.45 μm filtered air, until constant a weight. The samples were then homogenised by gently pressing with a stainless-steel spatula, avoiding grinding. Triplicate sub-samples (5 ± 0.02 g) from each slice were prepared for MP analysis.

MPs were analysed in accordance with the rapid screening method with Nile Red (Maes et al., 2017a), with slight modifications. Sediment subsamples were introduced into 50 mL centrifuge tubes with 30 mL of $ZnCl_2$ made to density 1.37 g mL^{-1}. 300 μL of NR stock solution (1 mg mL^{-1} in n-propanol) was then added, bringing the final concentration to 10 μg mL^{-1}. Samples were incubated for 30 min, re-suspending every 6 min to ensure maximum particle contact with the fluorophore, before being centrifuged (Thermo Scientific Heraeus Primo) for 5 min at 3900*g*. This aided the density separation of heavier and lighter particles in a shorter time (as described in Maes et al., 2017a supporting information). The resulting supernatant was transferred into clean centrifuge tubes and sediment-containing tubes were re-filled with $ZnCl_2$ and the steps of re-suspending, centrifuging and supernatant removal were repeated two more times. Due to high clay content, the supernatant $ZnCl_2$ from NWJB and CNYN samples was centrifuged further at 6000*g* for a period of 10 min.

The combined supernatant was then filtered onto 0.22 μm or 0.45 μm mixed cellulose ester or cellulose nitrate filters. The filters were transferred into glass petri dishes until imaging was complete and then stored for archiving in clean polystyrene petri dishes.

Imaging was carried out using a custom-made imaging rig (for details see supplementary Fig. S3/S5 and Table S2) following the method described in the Supporting Information of Maes et al. (2017a). Briefly, the head of a Motic trinocular microscope was mounted on a Sanven CNC3020T three-axis micro-milling/engraving machine and a Canon EOS 600D SLR camera was attached with a photomicroscope adaptor and used with shutter speed 1/5 s and ISO to 3200. A Kood orange filter (529 nm) was attached at the base of the microscope head and a blue crime light torch (420 - 470 nm, Foster and Freeman) was used to illuminate the whole filter area uniformly. The base of the imaging rig had a round aluminum holder constructed to house a 47 mm diameter filter. The imaging was controlled via Mach 3 (Artsoft) machine control software which had a G-code "toolpath" programmed to scan the filter area in a predefined mosaic, ensuring that each filter was imaged in the same way. The room light was dimmed, and external light sources kept to a minimum during imaging.

The fluorescent particles were identified from the resulting images and counted manually. The imaging conditions employed allowed detection of fluorescent objects down to 10 μm in size (determined using a stage micrometer). The fluorescent particles were classified into either 'particle' or 'fibre' categories, based on visual appearance (i.e., elongated appearance for fibre). Particles with any biological structures were considered as false positives and were excluded from the counts.

Initially, for IR-based cross-validation, only a very limited number of objects ($n = 19$) underwent spectroscopy. 12 were chosen as suspected plastic, 4 as suspected biological in origin and 3 fibres which did not fluoresce in the imaging step were included for the analysis as false negatives.

Items were analysed by FT-IR using a Thermo Scientific Nicolet iN10 MX at the Quadram Institute, Norwich. The instrument was controlled using the OMNIC Picta programme and set to a collection time of 22 s, 64 scans and high resolution. Background absorbance was taken from a blank area of a clean filter. To collect spectra, each item was located using the microscope on the instrument and an area of the object was selected and scanned with a 50 μm × 50 μm aperture. Interpretation of FT-IR spectra was carried out with KnowItAll® ID Expert from Bio-Rad with very conservative hit quality index (HQI) of greater than 80% selected.

Subsequently, a further 49 putative MPs were analysed in ATR mode using a Bruker Hyperion 2000 microscope, coupled with a Vertex 70 FT-IR spectrometer. The 20× Ge-tipped ATR lens was used for spectral acquisition and identities were assigned by spectral searching in a Bruker polymers database. Full details of this work can be found in supplementary information.

To determine the recovery rates, pre-extracted sediments ($n = 6$) were spiked with a known number of MPs obtained from the laboratory. The spiked samples contained 10 fragments of virgin polymethyl methacrylate (PMMA), 10 pieces of polyvinyl chloride (PVC), 10 pieces of sterile polystyrene (PS) petri dish (Sigma) and 10 pieces of nylon monofilament fishing line, MPs were created by cutting plastics into small fragments (approximately 0.5 - 2 mm along longest axis), using a clean scalpel blade. After sediments were spiked, samples were processed and imaged following the procedure detailed in the methods section. The method described above had a mean recovery rate of 100.5% for all particles and 67% for filaments.

Statistics were carried out with Microsoft Excel and the integrated development environment (IDE), RStudio version 1.1.414 (RStudio, Inc.) with significance threshold $\alpha = 0.05$. The median value from the three subsamples for each slice was used in the statistical analysis to represent the central tendency of fluorescent particles.

The relationship between total MP abundance in the sediment (particles and fibres) and the different environmental factors were analysed via generalised linear mixed model (GLMM) by using the 'glmer.nb' function of the lme4 package (Bates et al., 2015), with the influence of individual sediment cores treated as a random factor, to avoid pseudo-replication. Data were scaled and centred around zero (z values) for the GLMM, and the model was fitted with negative binomial error distribution. Residuals of the model were analysed to confirm homoscedasticity. Analysis of Cook's distances confirmed that there were no outliers influencing the model. Site specific GLMM was also applied at DB, but unfortunately there were too few cores from CNYN and NWJB to apply the GLMM model site-specifically and this could not be replicated at these locations.

To assess potential differences between the sites, the cores were normalised by considering only the top 10 cm of sediment to avoid dilution factor, as cores were different in length. A Kruskal-Wallis test was used to assess the difference between the locations in their MP-abundance.

3. Results

MPs ($n = 5687$) were found in all 22 sediment cores and 86.5% of all analysed 5 g subsamples ($n = 747$) contained MPs. However, only 6.7% ($n = 381$) were classified as fibres and just 29.0% ($n = 217$) of the 747 analysed subsamples across the three regions contained fibres. There was a significant difference in the number of fibres between the sites ($H = 44$, $df = 7$, $p < 0.05$), with DB having the highest occurrence of 15.2% ($n = 332$), whereas only 1.3% ($n = 20$) at NWJB and 1.2% ($n = 23$) at CNYN of MPs were fibres. The median MP abundance in the top 10 cm of sediment was also significantly different between the sites ($H = 48$, $df = 2$, $p < 0.05$) with 1.19 MP g^{-1} at DB, 1.05 MP g^{-1} at NWJB, 2.70 MP g^{-1} at CNYN. The GLMM model showed that MP concentrations significantly decreased with increasing sediment depth ($p < 0.05$, $z = -5.41$) (Fig. 2 & S2 for site specific GLMM) and increased with increasing water depth ($p < 0.05$, $z = 3.1$) (Fig. 3).

From the total 65 suspected MP particles that underwent spectroscopy, 66.1% were confirmed as MPs, with 15.3% of probable natural origin and 25.4% HQI < 60%/unidentified/no spectrum (Fig. 4). Multiple polymer types were present, with the most abundant being polyolefins (mostly polypropylene), paint, various polyamides, and polyester (PET) (Fig. 4). Selected examples of the FT-IR spectra are shown in Fig. 5, with 4 out of 4 suspected biological items confirmed as biological.

4. Discussion

MPs were found in all 22 sediment cores and MP abundance in the top 10 cm of sediments was estimated to be 1190 MP kg^{-1} dry weight (DW) at DB, 1050 MP kg^{-1} DW at NWJB and 2700 MP kg^{-1} DW at the CNYN. These findings are similar to previously reported ranges from oceanic sediments, such as, sediments of the China Yellow Sea (up to 4205 MP kg^{-1}) (Wang et al., 2019a) and Antarctic Peninsula (1300 MP kg^{-1}) (Cunningham et al., 2020), but are considerably lower than reported at the surface sediments of Baynes Sound and Lambert Channel in Canada (up to 25,000 MP kg^{-1}) (Kazmiruk et al., 2018). This highlights the heterogeneity of MP pollution across the world's oceans and emphasises the need for a much more comprehensive MP pollution baseline to be constructed.

If worst-case scenario MP concentrations are extrapolated across the area of each sample site, the top 10 cm of sediments may harbour up to 1.9×10^{15} MPs at Dogger bank (1.19 MP g^{-1}: 12331 km^2), 5.4×10^{13} MPs at the NWJB (1.05 MP g^{-1}: 399 km^2) and 2.3×10^{14} MPs at the CNYN area (2.7 MP g^{-1}: 661 km^2) (Area estimations retrieved from: JNCC, 2011; JNCC, 2013; JNCC, 2017). Although MP numbers were found to reduce progressively in deeper layers, MPs are still present, so these numbers could be an under-estimate of the total accumulation. These types of estimations, however, should be approached with caution, since spatial variance can be high, and extrapolations have been made based on a limited number of sites. Much higher spatial resolution would be required to fully estimate the extent of MP pollution within UK waters.

A relatively small fraction of MPs were fibres (6.7%), which is in

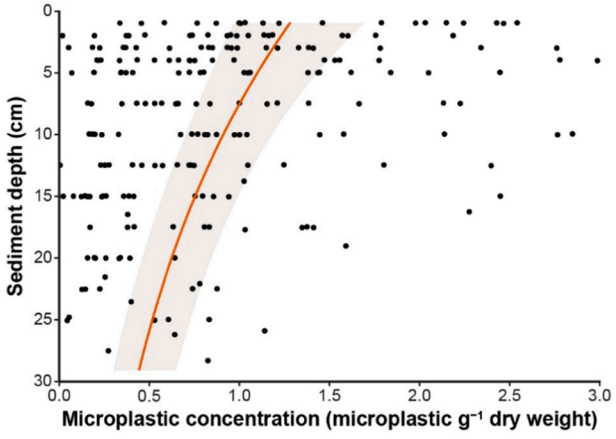

Fig. 2. Microplastic concentrations (microplastic g^{-1} dry weight) for all sediment samples plotted against sediment depth (cm). The red line shows the statistically significant negative relationship between the two variables ($p < 0.05$, $z = -5.41$), with shaded area representing 95% confidence interval. (For interpretation of the references to colour in this figure legend, the reader is referred to the web version of this article.)

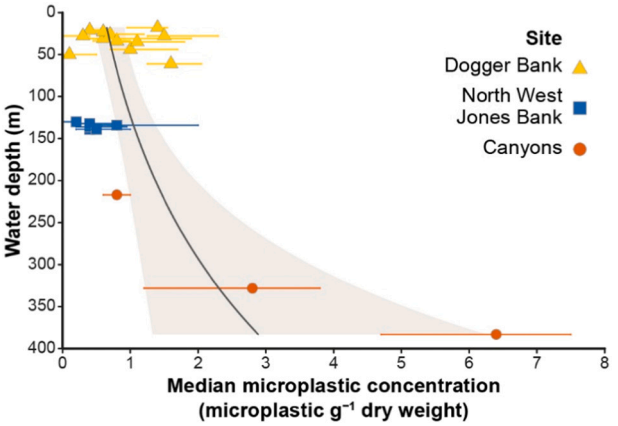

Fig. 3. Microplastic concentration (microplastic g^{-1} dry weight) plotted against water depth (m). Each point represents the median microplastic concentration of a sediment core, with error bars showing interquartile range. The black line shows the statistically significant positive relationship between the two variables ($p < 0.05$, $z = 3.1$), with shaded area representing 95% confidence intervals. Symbols and abbreviations: Dogger Bank: DB: yellow triangle, North West Jones Bank: NWJB: blue square and The Canyons: CNYN: red circle. (For interpretation of the references to colour in this figure legend, the reader is referred to the web version of this article.)

disagreement with most existing literature, where fibres have been identified as the most common morphology of MP in shelf environments, with the overall median value reported as ~64% based on 16 studies (Harris, 2020). Conversely, some studies have reported similar low percentages from the sediments (Kazour et al., 2019; Vianello et al., 2013). It is not clear which mechanism is driving these differences, but this could be a result of methodological differences, and/or be related to different sources and prevailing hydrological conditions at the sampled sites.

The current study had the lowest detection limit of 10 μm, enabling counting of more small particulate MPs, which could decrease the relative proportion of fibres. This suggests that the Nile Red protocol may overcome the observed phenomenon where visual counting with light microscopy can be biased towards fibres (Lenz et al., 2015). Conversely, it is also conceivable that Nile Red fails to stain all fibres present in the sample. Shim et al. (2016) found that PET dyed with Nile Red fluoresced weakly, and we have also noted relatively weak and variable staining of some model PET and PP fibres, although nylon generally stains reliably. Given that 70% of all plastic fibres ever made are made from polyester and the majority of this is PET (Geyer et al., 2017), this could potentially lead to underestimation. It is suggested that in future studies, each filter should be scanned twice: once under fluorescence conditions and once under brightfield illumination to capture any non-fluorescent fibres.

From the study sites, DB had a higher relative fibre abundance (15.2%) when compared with NWJB (1.3%) and CNYN (1.2%). This could partly reflect the effect of river outputs, atmospheric deposition, and prevailing hydrological conditions on the MP distribution. It has been shown that one of the major sources for synthetic fibres to the environment is from washing synthetic clothes in washing machines, which are then released into river systems (Dalla Fontana et al., 2020; Kärkkäinen and Sillanpää, 2021). As rivers ultimately flow into oceans, they have been regarded as a source of microfibres as well as macrolitter (Maes et al., 2018; Napper et al., 2021; Weideman et al., 2020), though whether they present a significant source of MPs to the deep oceans is still debated (Harris, 2020). Alternatively, microfiber abundance could be a result of atmospheric inputs. It has been shown that MPs, especially fibres, can be transported for long distances in the atmosphere (Allen et al., 2021; Evangeliou et al., 2020; Trainic et al., 2020; Wang et al., 2020b), and deposited to the oceans (Liu et al., 2019), thus the observed difference could be driven by winds. The UK is located at the area of converging air masses with prevailing wind direction from the north-east and south-west (Lapworth and McGregor, 2008). As DB would be affected mostly by polar continental air masses from Central Europe (Estellés et al., 2012: Met office 2022), it is conceivable that the air currents could carry more fibres than those affecting NWJB and CNYN which are affected mostly by maritime air masses (Estellés et al., 2012), which could be then deposited over the North Sea. These differences could be aggravated by hydrological conditions, as the area of the South-East edge of the UK continental shelf (NWJB and CNYN) is dominated by ocean currents flowing generally poleward (Pingree and Le Cann, 1989) and is an area of high mixing (Palmer et al., 2013), which could keep fibres in suspension and not allow deposition to occur. In contrast, the ocean currents at DB are weak and this might lead to more fibres being present in the lower velocity environment due to settling, similar to natural particles (Kane and Clare, 2019).

Another conceivable reason for a higher occurrence of fibres at DB could be the high fishing and maritime activity of the area which has been linked previously to higher fibre abundances (Ling et al., 2017; Vianello et al., 2013). It is possible that ropes and ghost nets (nets that have been left to drift in the Sea) degrade over time and shed these fibres, thus increasing their relative abundance, especially at DB where mixing is slow.

Distribution of MPs in the top 10 cm of the sediment varied between the sites. CNYN had the highest median MP abundance per gram of sediment and differed significantly from NWJB and DB. This dissimilarity might be linked to the respective water depth between the sites: water depth had a positive correlation with the MP abundance in the core samples ($p < 0.05$) and CNYN had the greatest water depth.

This is suspected to be related to the submarine canyons located at CNYN sampling sites, where near bottom currents carry nepheloid layers of particulate material to deeper waters (Wilson et al., 2015). Submarine canyons have previously been thought to be one of the oceanic transport mechanisms carrying MPs from shallows into the deeper sea, by acting as preferential conduits (Jones et al., 2022; Kane and Clare, 2019; Woodall et al., 2014), with turbidity currents being demonstrated to be capable of transporting MPs (Pohl et al., 2020). Similar phenomena of transportation of macrolitter from continental shelves through submarine canyons into the deep-sea environment also has been observed (Maes et al., 2018). The transportation from the shelf-break at the Celtic Sea to a depth of 1500 m is estimated to be about 1×10^6 cubic meters per second (Pingree and Le Cann, 1989), which could carry MP particles from the more turbulent NWJB area towards the continental shelf break and ultimately towards the deep sea. Although this study was not designed to address the sub-marine canyon transportation hypothesis, the results support this notation. However, to fully address how depth profile affects MP abundance, further studies where cores are collected with clear depth profiles from shallow to deeper waters is needed.

This study found that MP abundance decreases with increasing sediment depth ($p < 0.05$) and that MPs are present in the sediment down to a depth of 29 cm (Fig. 2), this agrees with existing literature (e.g. Willis et al., 2017; Zheng et al., 2020), where it has been reported that MP concentration decreases with increasing sediment depth. In contrast, a similar study at the Irish continental shelf reported no MPs in sediments below 3.5 ± 0.5 cm (Martin et al., 2017). This may be explained by the different analytical methods employed. Martin et al. (2017) sieved the samples with steel mesh which resulted in a lower size limit for MP detection of 250 μm, leading to a potential underestimation of smaller particles compared with the present study, which had a lowest detectable size at 10 μm. Furthermore, Nile Red was not used by Martin et al. (2017), which also could have led to an underestimation of MP particles in sediments.

The decrease of MP abundance with increasing sediment depth could possibly reflect the number of MPs in the environment at the time of deposition. If undisturbed, top sediments have been deposited more recently than those at deeper depths (Willis et al., 2017), thus rendering

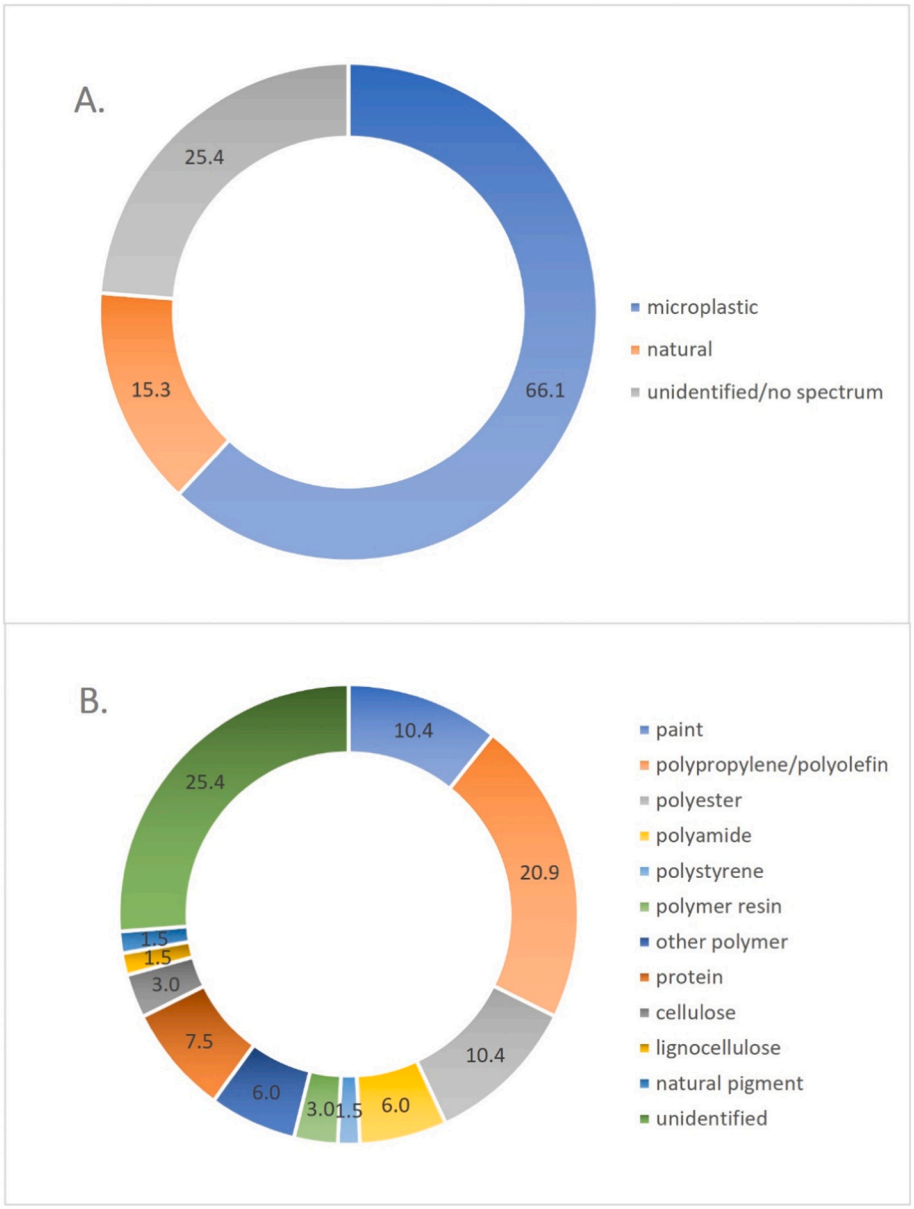

Fig. 4. Fraction of Nile Red positive particles identified as microplastics, natural materials or unidentified/no spectrum (A) and a breakdown of identified polymers (B). (For interpretation of the references to colour in this figure legend, the reader is referred to the web version of this article.)

sediments a proxy for temporal MP pollution trends. Determining the age of the sediments as a function of depth was out of the scope of this study and thus will not be discussed here further.

81.2% of particles positively identified by FT-IR spectroscopy were confirmed as synthetic polymers. Four suspected false positives were all confirmed by FT-IR to be biological in origin. Though a relatively low fraction of total MPs were spectroscopically analysed (about 1.2% from nearly 6000), these results suggest that the method used in the present study is effective in distinguishing between MP and potential false positives of natural origin. The latter might be further reduced by the introduction of an automated counting program with image recognition functions. It should be noted, however, that this approach carries an inherent risk, since smaller false biological positives may not be excluded, due to indistinguishable morphologies. Multiple particles, confirmed by FT-IR as biological, did not have a distinguishable biological morphology, demonstrating that a certain level of false positives does occur. Removal of biological material before the addition of Nile Red could provide further confidence in the method but could also lead to false negatives if digestion methods led to degradation of certain plastic types (Enders et al., 2016; Munno et al., 2018). This is an ever-present challenge in MP analysis, and transparency regarding the applied method and potential for false positives, false negatives, and systematic bias (e.g., by digesting small polyester particles/fibres) associated is imperative. Although much is discussed about false positives, very little focus has been placed on false negatives in Nile Red staining (either through methodological removal or non-staining), and a much greater understanding of this aspect is required and should be a focus in future research. Given the relatively low fraction of natural material identified, it may be preferable on cost and procedural grounds to avoid sample digestion, but further work will be needed in multiple sample types to confirm this.

This study processed a large sample set using the rapid screening method of Maes et al. (2017a), in real environmental samples, from three different locations, and assessed the efficiency of this method. The present study demonstrated that this technique is a practical and rapid way of processing and analyzing large quantities of samples (747

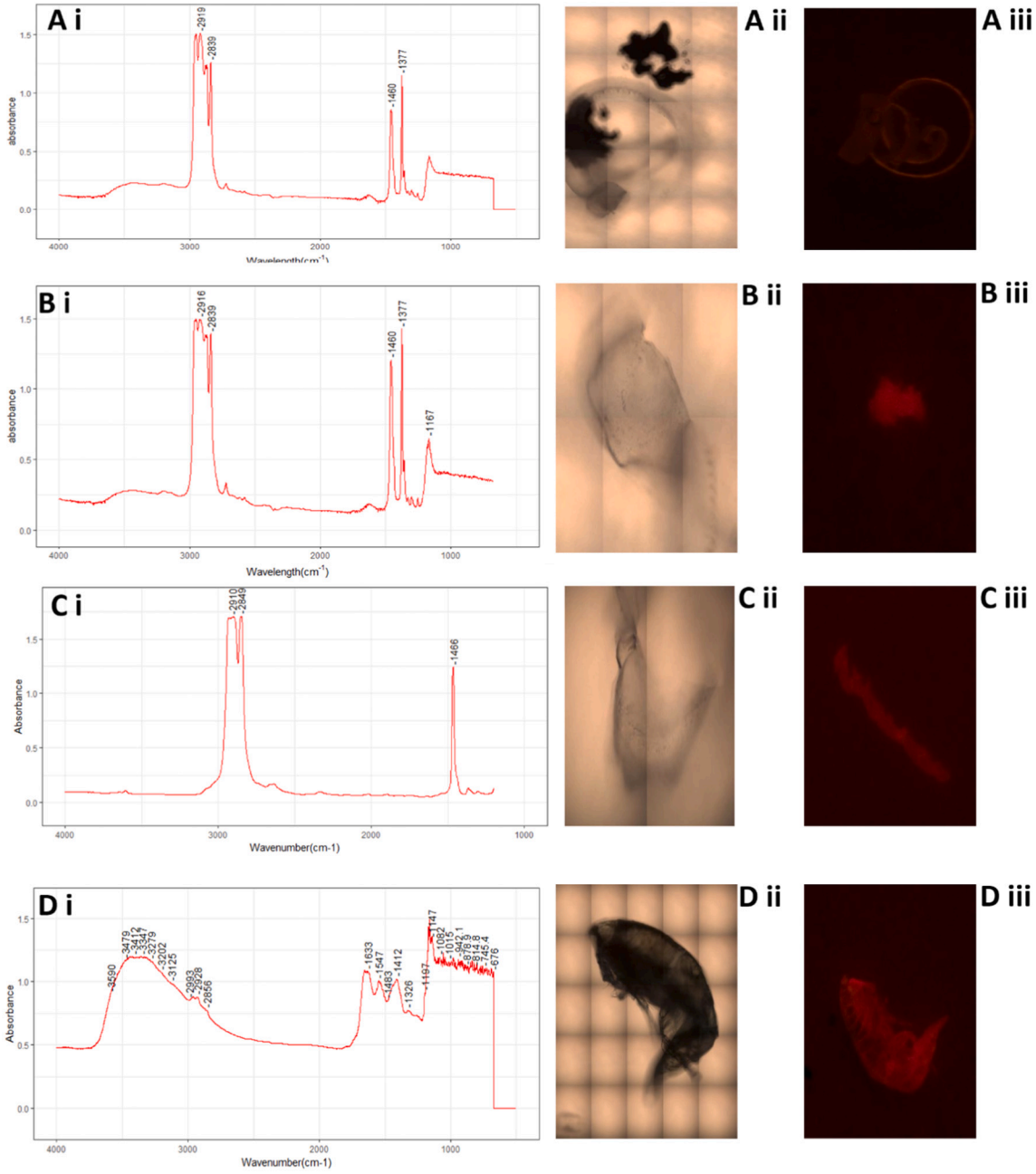

Fig. 5. Four representative examples of items collected for spectroscopy. *x*.i. Spectra collected from items picked for FT-IR analysis. *x*.ii. Bright field images of the objects *x*.iii. Images of objects under fluorescent conditions used during imaging: blue light (420–470 nm, Crimelite2 torch (Foster and Freeman)), through a 529 nm filter. A and B are polypropylene, C is ethylene-octene copolymer and D was confirmed as biological. (For interpretation of the references to colour in this figure legend, the reader is referred to the web version of this article.)

subsamples) within a relatively short time frame (13 weeks). Given that within this study, particles were manually counted from images, the rapid screening method displays great promise for the future. It is expected that when counting is undertaken by automated image analysis software (such as ImageJ), it will be possible to decrease the timescale of the data extraction even further. It has been demonstrated that ImageJ can be used in automated detection of MPs coupled with Nile Red staining (Prata et al., 2019). It might also be possible to discriminate common biological morphologies using automated image software (possibly with imaging in other spectral windows and modes, combined with AI for shape recognition), which could further reduce the occasional false positives generated by such structures. Overall, Nile Red provides a valuable method to reduce the subjective human bias (Löder et al., 2015).

Furthermore, the cost of building a custom-made imaging rig for rapid and consistent imaging and analysis was estimated to be ~£3000, plus a computer (see Supplementary Fig. S5 and Table S2 for details), making this method accessible for widespread usage, especially for laboratories which have limited access to state-of-the-art instrumentation (such as micro-FT-IR and Raman). The total recovery rates were also high (98.1–100.5%), giving confidence in the robustness of the method, though the fibre recovery rate stayed relatively low (67%). With modifications, such as, scanning the filters also under bright field, adaptation of the Nile Red method will allow the scientific community to move towards more objective and affordable ways of quantifying MPs from the environment.

5. Conclusion

MPs were recorded in 86.48% of all subsamples and none of the sediment cores analysed were MP free, highlighting the sheer magnitude of MP pollution in marine sediments. Different areas exhibited different fibre concentration, with DB having the highest concentration 15.2%. This may reflect riverine or atmospheric inputs to the area, which could be aggravated by hydrological conditions. MP abundance was found to increase with increasing water depth ($p < 0.05$), supporting the hypothesis that deeper water sediments act as a long-term sink for non-fibrous MPs. This may be due to active submarine canyons carrying MPs from shallow to deeper parts of the ocean. MP abundance also decreased with increasing sediment depth ($p < 0.05$), which could potentially represent the environmental concentrations of MPs, at the time of deposition. The screening method using Nile Red was found to be an efficient, rapid, and low-cost way of processing a large number of samples in a relatively short period, with relative accuracy and consistency. However, there is a need for further automation of the counting step from the images, and improved QA/QC via automated image recognition and artificial intelligence to improve data quality and confidence. Further cross-validation studies using vibrational spectroscopy will also give greater confidence and robust correction factors to improve the accuracy of quantitation. With such improvements implemented, the approach could provide an affordable, standardised method for monitoring and mapping in the future.

CRediT authorship contribution statement

Kukkola, A: conceptualization, investigation, methodology, formal analysis, visualization, writing- original draft, reviewing and editing. Senior, G: conceptualization, investigation, methodology, formal analysis, visualization, writing- reviewing and editing. Silburn, B: sampling and sediment resources, writing- reviewing. Bakir, A: formal analysis, reviewing. Maes, T: conceptualization, writing- reviewing. Kröger, S: conceptualization, supervision, project administration, writing-reviewing and editing. Mayes, A: conceptualization, methodology, supervision, project administration, funding acquisition, writing- reviewing and editing.

Data sharing

Data from this study can be accessed at: Kukkola *et al.*, Cefas (2022). Microplastics in sediment cores data from the UK continental shelf and slope 2017. Cefas, UK. V1. doi: https://doi.org/10.14466/CefasDataHub.129.

Declaration of competing interest

The authors declare that they have no known competing financial interests or personal relationships that could have appeared to influence the work reported in this paper.

Acknowledgements

The scientific staff and crew of the RV Cefas Endeavour CEND09/17 and CEND01/17 are gratefully acknowledged for their contribution to sample collection, as is the access to sample material provided by the partnership survey between Cefas and the JNCC as part of the Marine Protected Areas Programme.

The authors would also like to extend their gratitude towards Dr. Jon Sadler and Dr. Alexander Hurley for fruitful discussions regarding the statistical modelling and Dr. Holly Nel for inspirational discussions. The bathymetry used for the Fig. 1 was obtained from British Oceanographic Data Centre.

Funding

This work was supported by the Natural Environment Research Council NERC (grant number NE/S004831/1): University of East Anglia (UEA) and Centre for Environment, Fisheries and Aquaculture (Cefas). Thomas Maes received financial support from the Norwegian Agency for Development Cooperation, Ministry of Foreign Affairs (NORAD).

Appendix A. Supplementary data

Supplementary data to this article can be found online at https://doi.org/10.1016/j.marpolbul.2022.113554.

References

Allen, S., Allen, D., Baladima, F., Phoenix, V.R., Thomas, J.L., Le Roux, G., Sonke, J.E., 2021. Evidence of free tropospheric and long-range transport of microplastic at Pic du Midi observatory. Nat. Commun. 12 (1), 7242.

Araujo, C.F., Nolasco, M.M., Ribeiro, A.M.P., Ribeiro-Claro, P.J.A., 2018. Identification of microplastics using Raman spectroscopy: latest developments and future prospects. Water Res. 142, 426–440.

Bakir, A., Desender, M., Wilkinson, T., Van Hoytema, N., Amos, R., Airahui, S., Graham, J., Maes, T., 2020a. Occurrence and abundance of meso and microplastics in sediment, surface waters, and marine biota from the South Pacific region. Mar. Pollut. Bull. 160, 111572.

Bakir, A., van der Lingen, C.D., Preston-Whyte, F., Bali, A., Geja, Y., Barry, J., Mdazuka, Y., Mooi, G., Doran, D., Tooley, F., Harmer, R., Maes, T., 2020b. Microplastics in commercially important small pelagic fish species from South Africa. Front. Mar. Sci. 7 (910).

Bates, D.M., Bolker, M., Walker, B., S., 2015. Fitting linear mixed-effects models using lme4. J. Stat. Softw. 67 (1), 1–48.

Besseling, E., Foekema, E.M., Van Franeker, J.A., Leopold, M.F., Kühn, S., Bravo Rebolledo, E.L., Heße, E., Mielke, L., Ijzer, J., Kamminga, P., Koelmans, A.A., 2015. Microplastic in a macro filter feeder: humpback whale Megaptera novaeangliae. Mar. Pollut. Bull. 95 (1), 248–252.

Cunningham, E.M., Ehlers, S.M., Dick, J.T.A., Sigwart, J.D., Linse, K., Dick, J.J., Kiriakoulakis, K., 2020. High abundances of microplastic pollution in Deep-Sea sediments: evidence from Antarctica and the Southern Ocean. Environ. Sci. Technol. 54 (21), 13661–13671.

Cutroneo, L., Capello, M., Domi, A., Consani, S., Lamare, P., Coyle, P., Bertin, V., Dornic, D., Reboa, A., Geneselli, I., Anghinolfi, M., 2022. Microplastics in the abyss: a first investigation into sediments at 2443-m depth (Toulon, France). Environ. Sci. Pollut. Res. 29 (6), 9375–9385.

Dalla Fontana, G., Mossotti, R., Montarsolo, A., 2020. Assessment of microplastics release from polyester fabrics: the impact of different washing conditions. Environ. Pollut. 264, 113960.

Diesing, M., Ware, S., Foster-Smith, R., Stewart, H., Long, D., Vanstaen, K., Forster, R., Morando, A., 2009. Understanding the marine environment – seabed habitat investigations of the Dogger Bank offshore draft SAC. In: JNCC Report No. 429.

ECHA, E.C.A., 2019. Annex XV Restriction Report Proposal for a Restriction Substance Name(s): Intentionally Added Microplastics.

Eggett, A., McBreen, F., Griffiths, Y., van Rein, H., Last, E., Callaway, A., 2018. Report no 21. CEND0917 Cruise Report: North-West of Jones Bank and The Canyons Marine Conservation Zones' Monitoring Survey.

Enders, K., Lenz, R., Beer, S., Stedmon, C.A., 2016. Extraction of microplastic from biota: recommended acidic digestion destroys common plastic polymers. ICES J. Mar. Sci. 74 (1), 326–331.

Erni-Cassola, G., Gibson, M.I., Thompson, R.C., Christie-Oleza, J.A., 2017. Lost, but found with Nile red: a novel method for detecting and quantifying small microplastics (1 mm to 20 μm) in environmental samples. Environ. Sci. Technol. 51 (23), 13641–13648.

Estellés, V., Smyth, T.J., Campanelli, M., 2012. Columnar aerosol properties in a northeastern Atlantic site (Plymouth, United Kingdom) by means of ground based skyradiometer data during years 2000–2008. Atmos. Environ. 61, 180–188.

Geyer, R., Jambeck, J.R., Law, K.L., 2017. Production, use, and fate of all plastics ever made. Science Advances 3 (7). https://doi.org/10.1126/sciadv.1700782.

Harris, P.T., 2020. The fate of microplastic in marine sedimentary environments: a review and synthesis. Mar. Pollut. Bull. 158, 111398.

JNCC, 2011. Offshore Special Area of Conservation. Dogger Bank.

JNCC, 2013. In: Defra (Ed.), The Canyons Marine Conservation Zone Fact Sheet.

JNCC, 2017. In: Defra (Ed.), North-west of Jones Bank MPA.

Jones, E.S., Ross, S.W., Robertson, C.M., Young, C.M., 2022. Distributions of microplastics and larger anthropogenic debris in Norfolk Canyon, Baltimore Canyon, and the adjacent continental slope (Western North Atlantic Margin, U.S.A.). Marine Pollution Bulletin 174, 113047.

Kane, I.A., Clare, M.A., 2019. Dispersion, accumulation, and the ultimate fate of microplastics in deep-marine environments: a review and future directions. Front. Earth Sci. 7 (80).

Kärkkäinen, N., Sillanpää, M., 2021. Quantification of different microplastic fibres discharged from textiles in machine wash and tumble drying. Environ. Sci. Pollut. Res. 28 (13), 16253–16263.

Kazmiruk, T.N., Kazmiruk, V.D., Bendell, L.I., 2018. Abundance and distribution of microplastics within surface sediments of a key shellfish growing region of Canada. PLoS ONE 13 (5), e0196005.
Kazour, M., Jemaa, S., Issa, C., Khalaf, G., Amara, R., 2019. Microplastics pollution along the lebanese coast (Eastern Mediterranean Basin): occurrence in surface water, sediments and biota samples. Sci. Total Environ. 696, 133933.
Krause, S., Baranov, V., Nel, H.A., Drummond, J.D., Kukkola, A., Hoellein, T., Sambrook Smith, G.H., Lewandowski, J., Bonnet, B., Packman, A.I., Sadler, J., Inshyna, V., Allen, S., Allen, D., Simon, L., Mermillod-Blondin, F., Lynch, I., 2021. Gathering at the top? Environmental controls of microplastic uptake and biomagnification in freshwater food webs. Environ. Pollut. 268, 115750.
Kröger, S., Parker, R., Cripps, G., Williamson, P., 2018. Shelf Seas: The Engine of Productivity, Policy Report on NERC-Defra Shelf Sea Biogeochemistry programme. Cefas, Lowestoft.
Kröncke, I., Knust, R., 1995. The dogger Bank: a special ecological region in the Central North Sea. Helgoländer Meeresuntersuchungen 49 (1), 335–353.
Kukkola, A., Krause, S., Lynch, I., Sambrook Smith, G.H., Nel, H., 2021. Nano and microplastic interactions with freshwater biota – current knowledge, challenges and future solutions. Environ. Int. 152, 106504.
Lapworth, A., McGregor, J., 2008. Seasonal variation of the prevailing wind direction in Britain. Weather 63 (12), 365–368.
Lenz, R., Enders, K., Stedmon, C.A., Mackenzie, D.M.A., Nielsen, T.G., 2015. A critical assessment of visual identification of marine microplastic using raman spectroscopy for analysis improvement. Mar. Pollut. Bull. 100 (1), 82–91.
Ling, S.D., Sinclair, M., Levi, C.J., Reeves, S.E., Edgar, G.J., 2017. Ubiquity of microplastics in coastal seafloor sediments. Mar. Pollut. Bull. 121 (1), 104–110.
Liu, K., Wu, T., Wang, X., Song, Z., Zong, C., Wei, N., Li, D., 2019. Consistent transport of terrestrial microplastics to the ocean through atmosphere. Environ. Sci. Technol. 53 (18), 10612–10619.
Löder, M., Kuczera, M., Mintenig, S., Lorenz, C., Gerdts, G., 2015. Focal plane array detector-based micro-fourier-transform infrared imaging for the analysis of microplastics in environmental samples. Environ. Chem. 12 (5), 563–581.
Maes, T., Barry, J., Leslie, H.A., Vethaak, A.D., Nicolaus, E.E.M., Law, R.J., Lyons, B.P., Martinez, R., Harley, B., Thain, J.E., 2018. Below the surface: twenty-five years of seafloor litter monitoring in coastal seas of North West Europe (1992–2017). Sci. Total Environ. 630, 790–798.
Maes, T., Jessop, R., Wellner, N., Haupt, K., Mayes, A.G., 2017. A rapid-screening approach to detect and quantify microplastics based on fluorescent tagging with Nile Red. Scientific reports 7, 44501-44501.
Maes, T., Van der Meulen, M.D., Devriese, L.I., Leslie, H.A., Huvet, A., Frère, L., Robbens, J., Vethaak, A.D., 2017. Microplastics baseline surveys at the water surface and in sediments of the north-east Atlantic. Frontiers in Marine Science 4.
Maes, T., van Diemen de Jel, J., Vethaak, A.D., Desender, M., Bendall, V.A., van Velzen, M., Leslie, H.A., 2020. You are what you eat, microplastics in porbeagle sharks from the north east Atlantic: method development and analysis in spiral valve content and tissue. Frontiers in Marine Science 7 (273).
Martin, J., Lusher, A., Thompson, R.C., Morley, A., 2017. The deposition and accumulation of microplastics in marine sediments and bottom water from the Irish continental shelf. Scientific reports 7 (1), 10772-10772.
Noble-James, T., Jesus, A., McBreen, F., 2018. In: Monitoring Guidance for Marine Benthic Habitats, report no. 598. JNCC, Peterborough.
Office, Met. Air Mass Types. Retrieved from. https://www.metoffice.gov.uk/weather/learn-about/weather/atmosphere/air-masses/types.
Munno, K., Helm, P.A., Jackson, D.A., Rochman, C., Sims, A., 2018. Impacts of temperature and selected chemical digestion methods on microplastic particles. Environ. Toxicol. Chem. 37 (1), 91–98.
Murray, J., Holmes, I., Silburn, B., Sivyer, D., Pettigrew, J., S, S., Ware, S., 2017. Survey Report: CEND 01/17 Ecosystem Based Monitoring Case Study Southern North Sea: Dogger Bank Strata 2017.
Napper, I.E., Baroth, A., Barrett, A.C., Bhola, S., Chowdhury, G.W., Davies, B.F.R., Duncan, E.M., Kumar, S., Nelms, S.E., Hasan Niloy, M.N., Nishat, B., Maddalene, T., Thompson, R.C., Koldewey, H., 2021. The abundance and characteristics of microplastics in surface water in the transboundary Ganges River. Environ. Pollut. 274, 116348.
Napper, I.E., Davies, B.F.R., Clifford, H., Elvin, S., Koldewey, H.J., Mayewski, P.A., Miner, K.R., Potocki, M., Elmore, A.C., Gajurel, A.P., Thompson, R.C., 2020. Reaching new heights in plastic pollution—preliminary findings of microplastics on Mount Everest. One Earth 3 (5), 621–630.
Nel, H.A., Naidoo, T., Akindele, E.O., Nhiwatiwa, T., Fadare, O.O., Krause, S., 2021. Collaboration and infrastructure is needed to develop an African perspective on micro(nano)plastic pollution. Environ. Res. Lett. 16 (2), 021002.
Nielsen, T., Lokkegaard, B., Richardson, K., Pedersen, F.B., Hansen, L., 1993. Structure of plankton communities in the Dogger Bank area (North Sea) during a stratified situation. Mar. Ecol. Prog. Ser. 95, 115–131.
Palmer, M.R., Inall, M.E., Sharples, J., 2013. The physical oceanography of Jones Bank: a mixing hotspot in the Celtic Sea. Prog. Oceanogr. 117, 9–24.
Patchaiyappan, A., Dowarah, K., Zaki Ahmed, S., Prabakaran, M., Jayakumar, S., Thirunavukkarasu, C., Devipriya, S.P., 2021. Prevalence and characteristics of microplastics present in the street dust collected from Chennai metropolitan cityIndia. Chemosphere 269, 128757.
Pingree, R.D., Le Cann, B., 1989. Celtic and Armorican slope and shelf residual currents. Prog. Oceanogr. 23 (4), 303–338.
Prata, J.C., Reis, V., Matos, J.T.V., da Costa, J.P., Duarte, A.C., Rocha-Santos, T., 2019. A new approach for routine quantification of microplastics using Nile red and automated software (MP-VAT). Sci. Total Environ. 690, 1277–1283.
Preston-Whyte, F., Silburn, B., Meakins, B., Bakir, A., Pillay, K., Worship, M., Paruk, S., Mdazuka, Y., Mooi, G., Harmer, R., Doran, D., Tooley, F., Maes, T., 2021. Meso- and microplastics monitoring in harbour environments: a case study for the port of DurbanSouth Africa. Marine Pollution Bulletin 163, 111948.
Setälä, O., Fleming-Lehtinen, V., Lehtiniemi, M., 2014. Ingestion and transfer of microplastics in the planktonic food web. Environ. Pollut. 185, 77–83.
Shim, W.J., Song, Y.K., Hong, S.H., Jang, M., 2016. Identification and quantification of microplastics using Nile red staining. Mar. Pollut. Bull. 113 (1), 469–476.
Shruti, V.C., Pérez-Guevara, F., Roy, P.D., Kutralam-Muniasamy, G., 2022. Analyzing microplastics with Nile red: emerging trends, challenges, and prospects. J. Hazard. Mater. 423, 127171.
Silburn, B., 2018. In: Kukkola, A. (Ed.), Nioz Corer Information.
Sturm, M.T., Horn, H., Schuhen, K., 2021. The potential of fluorescent dyes—comparative study of Nile red and three derivatives for the detection of microplastics. Anal. Bioanal. Chem. 413 (4), 1059–1071.
Tamminga, M., Hengstmann, E., Fischer, E.K., 2018. Microplastic analysis in the south Funen archipelago, Baltic Sea, implementing manta trawling and bulk sampling. Mar. Pollut. Bull. 128, 601–608.
Thompson, C.E.L., Silburn, B., Williams, M.E., Hull, T., Sivyer, D., Amoudry, L.O., Widdicombe, S., Ingels, J., Carnovale, G., McNeill, C.L., Hale, R., Marchais, C.L., Hicks, N., Smith, H.E.K., Klar, J.K., Hiddink, J.G., Kowalik, J., Kitidis, V., Reynolds, S., Woodward, E.M.S., Tait, K., Homoky, W.B., Kröger, S., Bolam, S., Godbold, J.A., Aldridge, J., Mayor, D.J., Benoist, N.M.A., Bett, B.J., Morris, K.J., Parker, E.R., Ruhl, H.A., Statham, P.J., Solan, M., 2017. An approach for the identification of exemplar sites for scaling up targeted field observations of benthic biogeochemistry in heterogeneous environments. Biogeochemistry 135 (1), 1–34.
Valine, A.E., Peterson, A.E., Horn, D.A., Scully-Engelmeyer, K.M., Granek, E.F., 2020. Microplastic prevalence in 4 Oregon Rivers along a rural to urban gradient applying a cost-effective validation technique. Environ. Toxicol. Chem. 39 (8), 1590–1598.
Vianello, A., Boldrin, A., Guerriero, P., Moschino, V., Rella, R., Sturaro, A., Da Ros, L., 2013. Microplastic particles in sediments of lagoon of Venice, Italy: first observations on occurrence, spatial patterns and identification. Estuar. Coast. Shelf Sci. 130, 54–61.
Wang, J., Wang, M., Ru, S., Liu, X., 2019a. High levels of microplastic pollution in the sediments and benthic organisms of the South Yellow Sea, China. Sci. Total Environ. 651, 1661–1669.
Wang, W., Gao, H., Jin, S., Li, R., Na, G., 2019b. The ecotoxicological effects of microplastics on aquatic food web, from primary producer to human: a review. Ecotoxicol. Environ. Saf. 173, 110–117.
Weideman, E.A., Perold, V., Ryan, P.G., 2020. Limited long-distance transport of plastic pollution by the Orange-Vaal river system, South Africa. Sci. Total Environ. 727, 138653.
Willis, K.A., Eriksen, R., Wilcox, C., Hardesty, B.D., 2017. Microplastic distribution at different sediment depths in an urban estuary. Front. Mar. Sci. 4 (419).
Wilson, A.M., Raine, R., Mohn, C., White, M., 2015. Nepheloid layer distribution in the Whittard canyon, NE Atlantic margin. Mar. Geol. 367, 130–142.
Woodall, L.C., Sanchez-Vidal, A., Canals, M., Paterson, G.L.J., Coppock, R., Sleight, V., Calafat, A., Rogers, A.D., Narayanaswamy, B.E., Thompson, R.C., 2014. The deep sea is a major sink for microplastic debris. R. Soc. Open Sci. 1 (4).
Zhang, Q., Xu, E.G., Li, J., Chen, Q., Ma, L., Zeng, E.Y., Shi, H., 2020. A review of microplastics in table salt, drinking water, and air: direct human exposure. Environmental Science & Technology 54 (7), 3740–3751.
Zheng, Y., Li, J., Cao, W., Jiang, F., Zhao, C., Ding, H., Wang, M., Gao, F., Sun, C., 2020. Vertical distribution of microplastics in bay sediment reflecting effects of sedimentation dynamics and anthropogenic activities. Mar. Pollut. Bull. 152, 110885.